TOPOLOGICAL MATTER

Evidence for dispersing 1D Majorana channels in an iron-based superconductor

Zhenyu Wang[1,2], Jorge Olivares Rodriguez[1], Lin Jiao[1], Sean Howard[1], Martin Graham[3], G. D. Gu[4], Taylor L. Hughes[5], Dirk K. Morr[3], Vidya Madhavan[1]*

The possible realization of Majorana fermions as quasiparticle excitations in condensed-matter physics has created much excitement. Most studies have focused on Majorana bound states; however, propagating Majorana states with linear dispersion have also been predicted. Here, we report scanning tunneling spectroscopic measurements of crystalline domain walls (DWs) in $FeSe_{0.45}Te_{0.55}$. We located DWs across which the lattice structure shifts by half a unit cell. These DWs have a finite, flat density of states inside the superconducting gap, which is a hallmark of linearly dispersing modes in one dimension. This signature is absent in DWs in the related superconductor, FeSe, which is not in the topological phase. Our combined data are consistent with the observation of dispersing Majorana states at a π-phase shift DW in a proximitized topological material.

Majorana fermions are putative elementary particles that are their own antiparticles (*1*). Emergent analogs of these fermions have been argued to exist as quasiparticle excitations in condensed-matter systems (*2*–*7*) and have attracted much attention as possible building blocks of fault-tolerant quantum computation (*8*, *9*). So far, various predictions and realizations of localized Majorana bound states (MBS) have been reported. The platforms include strong spin-orbit–coupled semiconductor nanowires (*10*–*14*), ferromagnetic atomic chains (*15*–*17*), and topological insulators that are proximity-coupled with s-wave superconductors (*18*, *19*); in all of these cases, the MBS were spectroscopically identified as zero-energy conductance anomalies. In addition to the localized MBS, however, theoretical predictions show that dispersing Majorana states may also be realized as quasiparticles in condensed-matter systems (*18*, *20*–*22*). These quasiparticles are of fundamental interest and may be harnessed for quantum computing. Dispersive Majorana modes have been proposed as edge states of chiral p-wave superconductors, in hybrid systems that combine superconductors with a quantum anomalous Hall insulator (*23*), or two-dimensional (2D) magnetic Fe islands (*24*, *25*). However, these platforms are difficult to fabricate; moreover, most of them are stable only at low temperatures. This makes future applications highly challenging in these systems.

Iron-based superconductors provide an alternative pathway for pursuing Majorana modes at higher temperatures. $FeSe_xTe_{1-x}$ [Fe(Se,Te)] is the simplest compound in the Fe-based superconductor family, with an optimum critical temperature (T_c) of 14.5 K. This family of materials is highly attractive owing to its versatility and tunability. The materials grow well in thin film form (*26*), and their T_c can be substantially enhanced through doping, pressure, and strain (*27*). Through density functional theory, it has been found that for a range of concentrations around 50% Se, Fe(Se,Te) possesses helical Dirac surface states owing to band inversion along the Γ-*Z* direction (*28*–*31*). In accordance with the Fu and Kane model (*18*), when an s-wave superconducting gap opens in the Dirac surface states (because of proximity to s-wave superconductivity in the bulk), it provides the ideal conditions for hosting MBS. There are multiple pieces of supportive evidence for this scenario in Fe(Se,Te): High-resolution angle-resolved photoemission spectroscopy (ARPES) data reveal helical surface states that exhibit an s-wave gap below T_c, and a sharp zero-bias peak has already been observed inside vortex cores (*32*–*34*).

s-Wave–proximitized topological surface states can also host time-reversed pairs of dispersing 1D Majorana states along domain walls (DWs) separating regions in which the superconducting order parameter is phase-shifted by π (*18*). These modes possess a linear dispersion ($E = \pm v k_y$) with momentum parallel to the DW. This linear dispersion in one dimension implies a constant density of states (DOS) for energies below the superconducting gap—one of the key experimental signatures of dispersing Majorana states.

In this work, we used scanning tunneling microscopy (STM) to interrogate crystalline DWs in the proximitized Dirac surface states of $FeSe_{0.45}Te_{0.55}$ in a search for signatures of 1D dispersing Majorana modes.

As with most iron-based superconductors, the Fermi surface of $FeSe_{0.45}Te_{0.55}$ is composed of two hole pockets (Fig. 1A, α′ in red and β in green) around the Γ-point and two electron pockets (γ in blue) at the Brillouin zone corner (M-point). According to theory, Te substitution into FeSe shifts the bulk p_z band [found above the Fermi energy (E_F) in FeSe] downward toward the Fermi level (*29*). This band then hybridizes with the d_{xz} band (α band) to create a topological band inversion that pushes the α band ~14 meV below E_F. In the resulting band gap, a topological Dirac surface state emerges, centered at the Γ-point on the (001) surface (Fig. 1B). Below T_c, superconducting gaps are expected to open on both the surface and bulk bands (*32*).

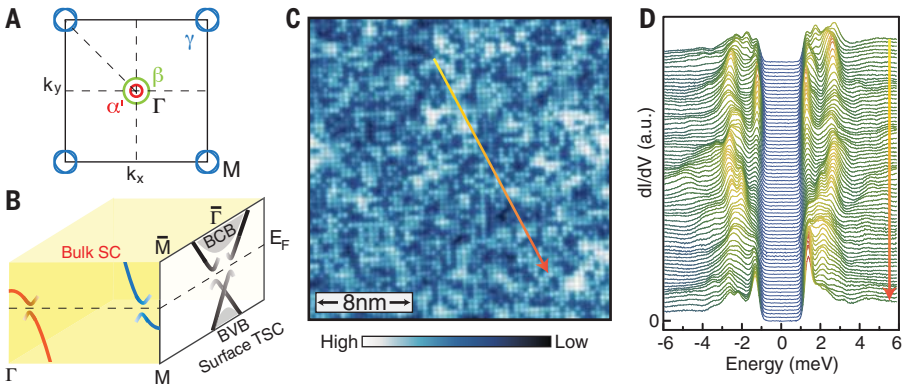

Fig. 1. Band structure and superconductivity in $FeSe_{0.45}Te_{0.55}$. (**A**) Sketch of bulk Fermi surfaces of Fe(Se,Te) at momentum $k_z = 0$. (**B**) Cartoon image showing superconductivity in the bulk and proximitized superconductivity in the topological surface state (*31*). (**C**) Topographic image in a 25- by 25-nm field of view (bias voltage V_S = 40 mV, tunneling current I_t = 100 pA). (**D**) Scanning tunneling spectroscopy (STS) data taken along the line shown in (C) at 0.3 K [V_S = 6 mV, I_t = 300 pA, modulation voltage (V_{mod}) = 58 μV]. The spectra are vertically offset for clarity.

[1]Department of Physics and Frederick Seitz Materials Research Laboratory, University of Illinois Urbana-Champaign, Urbana, IL 61801, USA. [2]Department of Physics, University of Science and Technology of China, Hefei, Anhui 230026, China. [3]Department of Physics, University of Illinois at Chicago, Chicago, IL 60607, USA. [4]Condensed Matter Physics and Materials Science Department, Brookhaven National Laboratory, Upton, NY 11973, USA. [5]Department of Physics and Institute for Condensed Matter Theory, University of Illinois at Urbana-Champaign, Urbana, IL 61801, USA.
*Corresponding author. Email: vm1@illinois.edu

In Fig. 1C, we show an atomically resolved STM topographic image of the chalcogen (Se/Te) surface layer, where the Te atoms appear brighter than Se because of their more extended electronic orbitals. There is a marked absence of interstitial Fe atoms on the surface, usually observed as bright protrusions in the topography (*35*, *36*). This, in combination with the sharp superconducting transition (fig. S1) (*37*), confirms the high quality of these samples. We measured a series of differential conductance (dI/dV) spectra along the line shown in Fig. 1C and present them in Fig. 1D. The data show that the spectral weight is completely suppressed to zero over a finite energy range ~±1 meV, and sharp peaks appear near the gap edge. These observations strongly suggest that there is no nodal structure in the gap function of $FeSe_{0.45}Te_{0.55}$, and the gap minima, if anisotropy exists, should be larger than 1 meV.

There is an ongoing controversy regarding the gap values for each band reported by various ARPES and optical conductivity studies on similar materials (*38*–*41*). STM is the ideal probe with which to measure gap values on different bands with high accuracy. However, because of the inhomogeneity caused by doping in Fe(Se,Te), the gap values and thus the number of gaps seen in any one spectrum show spatial variations (Fig. 1D). To obtain statistical information on the gap values and distribution, we recorded tunneling spectra $dI(r, V)/dV$ on a densely spaced grid (240 by 240) over a 100- by 100-nm field of view (FOV). The gap values were extracted through our multigap-finding algorithm, which finds the position of peak and shoulder features in each dI/dV spectrum and accepts them as coherence peaks if they are particle-hole symmetric (*37*). We classify the results by the number of gaps found for each spectrum and show a color-coded 2D map (gap map) in Fig. 2A.

We found spectra with one, two, or three gaps in the energy range (–3.5 meV, 3.5 meV). To visualize the evolution of the spectra as a function of position, a spectral line cut traversing the three regions (white line on the gap map) is shown in Fig. 2B. One can see the spectra evolving from displaying two gaps to three and then to a single gap. The statistical analysis of the gap magnitudes divided by category (colored histograms), as well as the overall results, are shown in Fig. 2C. For ~20% of the spectra taken in this FOV, we can distinguish only one gap centered around 1.4 meV; the two-gap spectra cover ~57% of the FOV area, with mean gap values around 1.4 and 2.4 meV; in the remaining area, three gaps can be detected simultaneously, with mean values of 1.4, 1.9, and 2.4 meV. These data suggest that multiple gaps exist at all points of the sample, but statistical variations in their magnitude sometimes prevent us from resolving them individually. The largest gap value extracted from ARPES is around 4 to 5 meV (*40*). This larger gap is only seen as a hump-like feature in our spectra and was not picked up in our gap map because of the suppressed intensity of the corresponding peaks. However, this feature can be seen in line cuts (fig. S2) (*37*). If we assign this hump-like feature (around ±4.5 meV) to be the coherence peaks arising from the large superconducting gap on the γ sheet as shown in (*40*), then, by comparison with ARPES data, the mean gap values of 1.4 and 2.4 meV may be assigned to the smaller gaps on the α′ and β bands, respectively. This suggests that consistent with recent ARPES data, the 1.9-meV gap may be assigned to the topological surface state, indicating the topological nature of these samples (*32*).

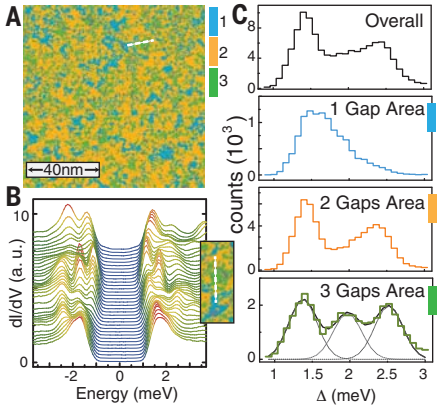

Fig. 2. Statistical analysis of superconducting gaps. (**A**) 100- by 100-nm map depicting the distribution of superconducting gaps in $FeSe_{0.45}Te_{0.55}$. Blue, orange, and green colors indicate whether a single gap, two gaps, or three gaps were found at each pixel, respectively. The gap values at each pixel were obtained through a multipeak-finding algorithm (37). (**B**) STS spectra at 0.3 K obtained along the white line shown in (A), starting (top to bottom) with a two-gap region (orange), which transitions to a three-gap region (green) and ends in a single-gap region (blue). The spectra are vertically offset for clarity. (**C**) Histogram of the gap values in the one-, two-, and three-gap regions. The dark curves show Gaussian fits to the gap distribution, with mean gap values of 1.4, 1.9, and 2.4 meV.

Recent STM measurements in Fe(Se,Te) have reported the existence of zero-bias conductance peaks inside vortex cores and near interstitial Fe atoms (*33*, *34*, *36*), which have been proposed to be signatures of zero-dimensional MBS. We observed similar spectral line shapes inside several vortex cores and near–atomic-scale defects (figs. S3 and S4) in our samples, all of which are consistent with a topologically nontrivial surface state (*37*). Here, we report the existence of 1D dispersing Majorana modes near a domain-wall defect. This defect was discovered with atomically resolved topography as a 1D feature on the surface represented by a bright line (Fig. 3A). A zoomed-in view (Fig. 3D) reveals that this bright line separates two crystal domains where the lattice shows a relative phase shift. This shift is reflected as a split in reciprocal-space Bragg peaks of the Fourier transform of the image (Fig. 3B and fig. S5) (*37*). The magnitude of the split in reciprocal space corresponds to a spatial scale of 12 nm (half of the FOV of Fig. 3A), which is consistent with the domain size in this FOV. To determine the magnitude of the lattice shift between the two sides of the DW, we carried out a displacement analysis (fig. S6), which maps the relative phase of the lattice on either side (*37*). The analysis indicates that the lattice undergoes a half-unit-cell shift across such a DW. This half-unit-cell shift, as we will show later, is essential for the realization of dispersing Majorana modes.

Differential conductance spectra obtained along three distinct paths traversing the DW (Fig. 3F) reveal an intriguing evolution. As one approaches the DW, the superconducting coherence peaks in the dI/dV spectra are suppressed, and new electronic states emerge inside the gap, resulting in a nearly featureless, constant finite dI/dV inside the gap at the DW center as indicated with the highlighted lines in Fig. 3F and the inset (fig. S7) (*37*). Despite the constant DOS inside the superconducting gap, the DOS at the DW still exhibits superconducting signatures (Fig. 3F, inset, and fig. S8H) , which indicates that the flat DOS is not simply caused by a region of normal metal (*37*). One explanation for this observation is the presence of linearly dispersing Majorana states at the DW because it would naturally give rise to a constant dI/dV in one dimension.

According to the Fu-Kane model (*18*), realizing 1D dispersing Majorana states requires three ingredients: nontrivial topological surface states, s-wave superconductivity that gaps the surface states, and a π-phase shift in the superconducting order parameter across the DW. Our detailed gap maps already indicate the presence of proximity-gapped Dirac surface states, thus satisfying the first two criteria. This leaves us with the question of how to generate a superconducting phase shift. For the pairing symmetries allowed in Fe(Se,Te), it is possible to have an interplay between the crystal structure and the phase of the superconducting order parameter. One possibility comes from the predicted odd parity s-wave pairing in iron-based superconductors, which encodes pairing between next-nearest-neighbor sites (*42*, *43*) in the 2-Fe unit cell. In this case, the order parameters on the two Fe-sublattices have a π-phase difference. A half-unit-cell shift of the lattice in such a system would naturally create a π-phase shift across the domains (Fig. 3E). It has also been argued that the s± pairing in iron-based superconductors can

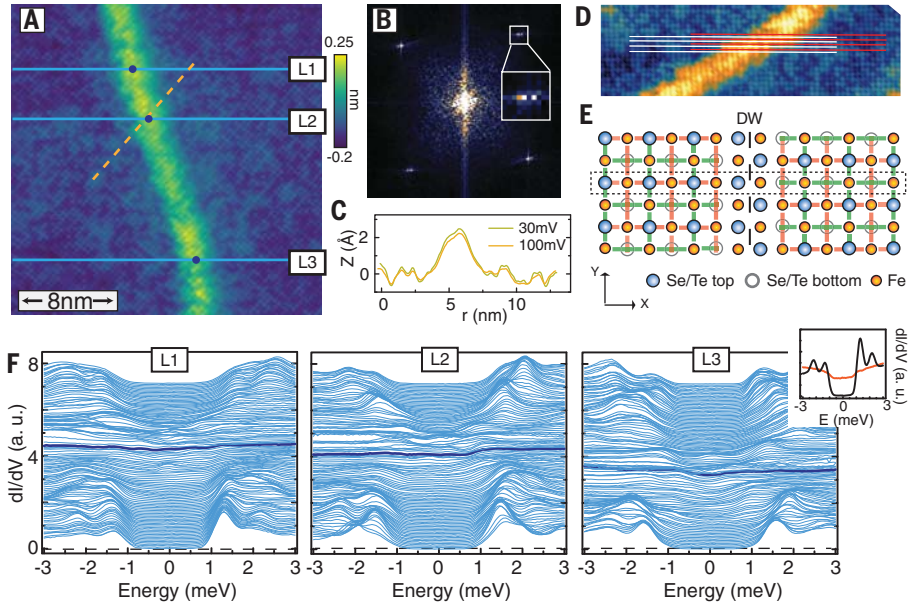

Fig. 3. Signature of dispersing 1D Majorana modes at a DW. (**A**) 25- by 25-nm topographic image showing a DW (bright line) (V_S = 4 mV, I_t = 250 pA). (**B**) 2D fast Fourier transform of (A), showing a splitting of the Bragg peaks, which indicates the presence of domains in this image. (Inset) Zoom-in near one of the Bragg peaks. (**C**) Height scans taken at different bias voltages along the yellow dashed line in (A). (**D**) Zoom-in of the DW. The white and red lines track the atomic lattice on both sides of the DW. A half-unit-cell shift can be observed between one side and the other. (**E**) Schematic of the half-unit-cell shift across the DW. The schematic also depicts how one might obtain a π-phase shift in the superconducting order parameter across such a DW. Superimposed on the lattice are red and green bars, which denote the parity of next-nearest-neighbor pairing (*42*, *43*). As an example, tracking the atoms inside the dashed box, one can see that the parity shifts from red on the left of the DW to green on the right. This creates a π-phase shift in the superconducting order parameter. (**F**) Line-cut profiles of *dI/dV* spectra along the three blue lines in (A), which cross the DW (V_S = 4 mV, I_t = 250 pA, V_{mod} = 58 μV). The spectra shapes obtained right on the DW [at position of dots in (A)] are highlighted with a dark blue color. For clarity, the spectra are vertically offset from each other by 0.06 (6 nS). (Inset) A direct comparison of the spectra taken on the DW (orange) and far away (black). All data were obtained at 0.3 K.

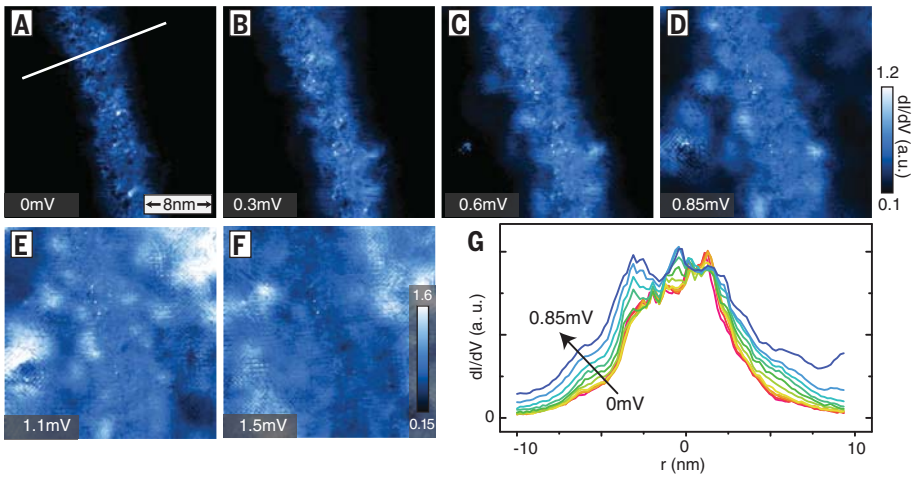

Fig. 4. Spatial distribution of the 1D Majorana mode at a DW with increasing energy. (**A** to **F**) *dI/dV* maps from 0 to 1.5 meV at 0.3 K. The maps are 25 by 25 nm in size, and spectra were obtained on a 130- by 130-pixel grid. DW states are present at all energies inside the gap up to 1 meV, when the states merge into the coherence peaks. However, the spatial extent of the states grows with increasing energy. (**G**) DOS profiles measured at different energies along the white line perpendicular to the DW.

generate a π-phase shift at the intersections of crystal terminations with different orientations (*44*). Thus, Fe(Se,Te) is an excellent candidate, with all the essential ingredients necessary for hosting dispersing Majorana modes.

To distinguish this possibility from other scenarios, we studied other extended defects (figs. S9 and S10) that are not expected to give rise to a π-phase shift and found that the flat DOS signature is absent (*37*); 1D defects without the half-unit-cell shift have the effect of decreasing the gap magnitude (fig. S9), whereas step edges, which are strong potential scatterers, induce resonant bound states inside the superconducting gap (fig. S10). Furthermore, the half-unit-cell shift DW is spectroscopically similar to the rest of the sample above T_c. As shown in fig. S8, at 14 K the spectra both on and away from the DW are almost identical (*37*). This indicates that the DW does not have a noticeable effect on the local electronic structure above T_c, and its effects become prominent only below T_c.

One might wonder whether the experimentally observed DW modes could also possess a topologically trivial origin, unrelated to existence of a topological surface state. On the basis of previous studies, the superconducting order parameter in Fe(Se,Te) is expected to be a sign-changing s± state (*45*, *46*). In such a state, defects, regardless of their magnetic properties, would induce impurity states inside the superconducting gap. The experimentally observed DW representing a 1D defect could therefore lead to the emergence of an impurity band inside the superconducting gap even in a topologically trivial phase. To investigate this possibility, we used a theoretical model for a topologically trivial superconducting state of Fe(Se,Te) (*47*) and represented the DW as a line of potential scatterers (fig. S11) (*37*). We found, as expected, that the DW gives rise to impurity states inside the superconducting gap. However, these states do not in general traverse the superconducting gap (only for fine-tuned values of the scattering potential do impurity states near zero energy emerge). Moreover, such states are not uniformly distributed in energy inside the gap and cannot result in the observed constant density of states. The same conclusion holds if the DW-separated, π-phase–shifted superconducting regions are present in an otherwise topologically trivial phase (fig. S12) (*37*). These findings are further confirmed by our experimental study of twin DWs in the topologically trivial but related superconducting compound, FeSe (fig. S13) (*37*). Although such DWs give rise to a suppression of the superconducting gap, they do not result in a constant DOS. These theoretical and experimental findings taken together make it unlikely that the observed constant DOS near the DW can arise in a topologically trivial superconducting phase, which

further emphasizes the important role played by nontrivial topology in creating the observed DW modes.

The topological nature of the DW modes necessarily dictates a specific spatial and energy dependence of the DW states. In particular, with increasing energy, the Majorana mode must continuously evolve from being localized at the DW at zero energy to being delocalized as their energy reaches the gap edge. In other words, the modes' localization length increases with increasing energy, leading to an increase in the modes' spatial extent from the DW. To visualize this evolution, we obtained spatial differential conductance maps (dI/dV maps) in the vicinity of the DW ranging in energies from E_F up to 1.5 mV, where the first set of coherent peaks is located (Fig. 4, A to F). At E_F, the in-gap states are confined within an ~3-nm width. These states begin to expand in real space with increasing energy and become far less visible at 0.85 mV because of a lack of contrast in the intensity with respect to the rest of the area. The dI/dV maps show that the DW states are present at all energies inside the gap. However, the spatial extent of the states grows with increasing energy, which is consistent with a topological origin for these modes.

$FeSe_{0.45}Te_{0.55}$ may have provided the first glimpse into linearly dispersing 1D Majorana modes. Possible future experiments include the measurement of the fractional (4π) Josephson effect using a flux loop or depositing magnetic layers to generate chiral Majorana modes or localized MBS. Beyond the Majorana fermion context, our experimental results have two important implications. First, our observations provide supporting evidence for the existence of topological surface states and a Fu-Kane proximitized superconducting state in $FeSe_{0.45}Te_{0.55}$. Second, the connection between the crystal DW and the superconducting π-phase shift provides evidence in support of a superconducting order parameter with a real-space sign change within a unit cell (*42*).

REFERENCES AND NOTES

1. E. Majorana, *Nuovo Cim.* **14**, 171–184 (1937).
2. N. Read, D. Green, *Phys. Rev. B* **61**, 10267–10297 (2000).
3. A. Kitaev, *Ann. Phys.* **321**, 2–111 (2006).
4. D. A. Ivanov, *Phys. Rev. Lett.* **86**, 268–271 (2001).
5. J. Alicea, *Rep. Prog. Phys.* **75**, 076501 (2012).
6. C. W. J. Beenakker, *Annu. Rev. Condens. Matter Phys.* **4**, 113–136 (2013).
7. S. R. Elliott, M. Franz, *Rev. Mod. Phys.* **87**, 137–163 (2015).
8. A. Kitaev, *Ann. Phys.* **303**, 2–30 (2003).
9. C. Nayak, S. H. Simon, A. Stern, M. Freedman, S. Das Sarma, *Rev. Mod. Phys.* **80**, 1083–1159 (2008).
10. R. M. Lutchyn, J. D. Sau, S. Das Sarma, *Phys. Rev. Lett.* **105**, 077001 (2010).
11. Y. Oreg, G. Refael, F. von Oppen, *Phys. Rev. Lett.* **105**, 177002 (2010).
12. V. Mourik *et al*., *Science* **336**, 1003–1007 (2012).
13. A. Das *et al*., *Nat. Phys.* **8**, 887–895 (2012).
14. S. M. Albrecht *et al*., *Nature* **531**, 206–209 (2016).
15. S. Nadj-Perge *et al*., *Science* **346**, 602–607 (2014).
16. M. Ruby *et al*., *Phys. Rev. Lett.* **115**, 197204 (2015).
17. H. Kim *et al*., *Sci. Adv.* **4**, eaar5251 (2018).
18. L. Fu, C. L. Kane, *Phys. Rev. Lett.* **100**, 096407 (2010).
19. H. H. Sun *et al*., *Phys. Rev. Lett.* **116**, 257003 (2016).
20. A. P. Schnyder, S. Ryu, A. Furusaki, A. W. W. Ludwig, *Phys. Rev. B* **78**, 195125 (2008).
21. X. L. Qi, T. L. Hughes, S. Raghu, S.-C. Zhang, *Phys. Rev. Lett.* **102**, 187001 (2009).
22. Y. Tanaka, M. Sato, N. Nagaosa, *J. Phys. Soc. Jpn.* **81**, 011013 (2012).
23. Q. L. He *et al*., *Science* **357**, 294–299 (2017).
24. S. Rachel, E. Mascot, S. Cocklin, M. Vojta, D. K. Morr, *Phys. Rev. B* **96**, 205131 (2017).
25. A. Palacio-Morales *et al*., *Sci. Adv.* **5**, eaav6600 (2019).
26. P. Mele, *Sci. Technol. Adv. Mater.* **13**, 054301 (2012).
27. K. Horigane, N. Takeshita, C.-H. Lee, H. Hiraka, K. Yamada, *J. Phys. Soc. Jpn.* **78**, 063705 (2010).
28. N. Hao, J. Hu, *Phys. Rev. X* **4**, 031053 (2014).
29. Z. Wang *et al*., *Phys. Rev. B* **92**, 115119 (2015).
30. X. Wu, S. Qin, Y. Liang, H. Fan, J. Hu, *Phys. Rev. B* **93**, 115129 (2016).
31. G. Xu, B. Lian, P. Tang, X.-L. Qi, S.-C. Zhang, *Phys. Rev. Lett.* **117**, 047001 (2016).
32. P. Zhang *et al*., *Science* **360**, 182–186 (2018).
33. D. Wang *et al*., *Science* **362**, 333–335 (2018).
34. T. Machida *et al*., *Nat. Mater.* **18**, 811–815 (2019).
35. M. Chen *et al*., *Nat. Commun.* **9**, 970 (2018).
36. J. Yin *et al*., *Nat. Phys.* **11**, 543–546 (2015).
37. Materials and methods are available as supplementary materials.
38. B. Zeng *et al*., *Nat. Commun.* **1**, 112 (2010).
39. K. Okazaki *et al*., *Phys. Rev. Lett.* **109**, 237011 (2012).
40. H. Miao *et al*., *Phys. Rev. B* **85**, 094506 (2012).
41. C. C. Homes *et al*., *J. Phys. Chem. Solids* **72**, 505–510 (2011).
42. J. Hu, *Phys. Rev. X* **3**, 031004 (2013).
43. N. Hao, J. Hu, *Phys. Rev. B* **89**, 045144 (2014).
44. R. X. Zhang, W. S. Cole, S. Das Sarma, *Phys. Rev. Lett.* **122**, 187001 (2019).
45. T. Hanaguri, S. Niitaka, K. Kuroki, H. Takagi, *Science* **328**, 474–476 (2010).
46. P. J. Hirschfeld, M. M. Korshunov, I. Mazin, *Rep. Prog. Phys.* **74**, 124508 (2011).
47. S. Sarkar *et al*., *Phys. Rev. B* **96**, 060504 (2018).
48. Z. Wang *et al.*, Replication data for: Evidence for dispersing 1D Majorana channels in an iron-based superconductor. Zenodo (2019); 10.5281/zenodo.3529111

ACKNOWLEDGMENTS

The authors thank H. Ding, S. Kivelson, and C. Kane for useful conversations. **Funding:** The work in Brookhaven is supported by the Office of Science, U.S. Department of Energy, under contract DE-SC0012704. V.M. gratefully acknowledges support from U.S. Department of Energy, Office of Science, Basic Energy Sciences, under award DE-SC0014335 (STM studies) and NSF award DMR-1610143. T.L.H. thanks the U.S. National Science Foundation under the Materials Research Science and Engineering Center program under NSF award DMR-1720633 (SuperSEED) for support. M.G. and D.K.M. acknowledge support from the U.S. Department of Energy, Office of Science, Basic Energy Sciences, under award DE-FG02-05ER46225. **Author contributions:** V.M. and Z.W. conceived the experiments; Z.W., J.O.R., and L.J. performed the experiments; J.O.R. and S.H. wrote software for data analysis; Z.W., J.O.R., and S.H. carried out data analysis; G.D.G. made the samples; M.G., T.L.H., and D.K.M. carried out the theory; and V.M. and Z.W. wrote the paper, with contributions from all authors. **Competing interests:** The authors declare no competing interests. **Data and materials availability:** The experimental data and theory code of this study are available at (*48*).

SUPPLEMENTARY MATERIALS

science.sciencemag.org/content/367/6473/104/suppl/DC1
Materials and Methods
Supplementary Text
Figs. S1 to S13
Tables S1 and S2
References (*49*, *50*)

29 January 2019; resubmitted 20 July 2019
Accepted 14 November 2019
10.1126/science.aaw8419

Science

Evidence for dispersing 1D Majorana channels in an iron-based superconductor

Zhenyu Wang, Jorge Olivares Rodriguez, Lin Jiao, Sean Howard, Martin Graham, G. D. Gu, Taylor L. Hughes, Dirk K. Morr and Vidya Madhavan

Science **367** (6473), 104-108.
DOI: 10.1126/science.aaw8419

A possible propagating Majorana

Majorana states in solid-state systems may one day form a basis for topological quantum computing. Most of the candidates identified so far have been Majorana bound states, but theorists have predicted that propagating Majorana states may exist as well. Wang *et al.* looked for such a state on the surface of the material $FeSe_{0.45}Te_{0.55}$ (see the Perspective by Tewari and Stanescu). Using scanning tunneling spectroscopy, the researchers measured a flat, bias-independent density of states along a particular type of domain wall, which was consistent with a theoretical prediction for a propagating Majorana state in this material. Although topologically trivial origins of this finding are difficult to completely rule out, the work is likely to stimulate interest in iron-based superconductors as hosts of Majorana states.

Science, this issue p. 104; see also p. 23

Science (print ISSN 0036-8075; online ISSN 1095-9203) is published by the American Association for the Advancement of Science, 1200 New York Avenue NW, Washington, DC 20005. The title *Science* is a registered trademark of AAAS.